Chime, A. C., Bensmida, S., Chakaroun, M., Lee, M. W., Nkwawo, H., & Fischer, A. P. A. (2018). Electrical modelling and design of ultra-fast micro-OLED with coplanar wave-guided electrodes in ON-OFF regime. *Organic Electronics*, *56*, 284-290. https://doi.org/10.1016/j.orgel.2017.12.026

# Electrical modelling and design of ultra-fast micro-OLED with coplanar wave-guided electrodes in ON-OFF regime

A. C. Chime, S. Bensmida, M. Chakaroun, M. W. Lee, H. Nkwawo, A. P. A. Fischer

**This work proposes a new electrical model and design of ultra-fast µ-OLED devices under ON-OFF electrical pulse regime. The new model is an equivalent electrical model capable of accounting for large amplitude excitation as well as ultra-short pulse response. Moreover, coplanar wave-guided electrodes are proposed, for the first time, to maximize pulse energy delivery to the organic hetero-structure and to minimize the µ-OLED time response. An analytical expression of the time response is derived from the model which reveals the design key parameters. Moreover, preliminary experimental results presented in this work demonstrate state-of-the-art OLED current density of 2kA/cm$^2$ and better than state-of-the-art optical pulse duration as short as 10 ns in the range of the radiative lifetime of singlet excitons.**

**Introduction:**

Organic Light Emitting Diodes (OLEDs) are mainly and largely exploited in display and lighting applications. However, in the field of organic opto-electronics, the demonstration of the organic laser diode remains one of the most important challenge. The main obstacles to achieve lasing with organic semiconductors under electrical pumping are; the low mobility in organic semiconductors, heating, several loss mechanisms due to injected charges, exciton formation, and high laser-threshold level [1, 2].

High current density is one of the requirements to reach the laser threshold excitation level [3, 4]. Such high excitation levels require extremely high charges densities. This leads to additional absorption losses that are the result of undesired annihilation processes (in particular singlet-polaron and singlet-triplet quenching) [1, 5, 6, 7]. As triplets do not contribute to the lasing process and have long excited state lifetime, they quickly accumulate in the gain medium and become detrimental to the laser effect. This phenomenon can be avoided in the presence of very short pulsed excitation. This can be achieved by choosing a pulse duration that is short enough so that the triplet population does not become significant before the end of the pulse and by adjusting the repetition rate (or the duty cycle) such that there is sufficient time for triplet relaxation between successive pulses [7]. In other words, the pulse duration should be less than the lifetime of the singlet states (The radiative lifetime of singlet excitons being in the range from 0.2 to 20 ns)[8], while the repetition period should be greater than the relaxation time of the triplet states. Additionally, a small active area device should lead to low sample capacitance, and hence, fast response time [9]. Short pulse duration should therefore result in avoiding exciton annihilation and, hence, could lead to better external quantum efficiency (EQE) [10, 11, 3, 12]. Moreover, under these conditions of high density of excitation, better heat management may lead to higher current densities [1, 9, 13].

Recently, significant research efforts reported OLED responses under pulsed electrical excitation regime [1, 9, 14, 15]. To the best of authors knowledge, the shortest pulse durations were reported in [1,15] with 50ns pulse. Shorter pulses require a large bandwidth impedance matching circuit so that the energy of the electrical pulse is effectively transmitted to the component. This last aspect was omitted in previously reported work.

In this paper, a new OLED equivalent electrical model is proposed and developed for ON-OFF operation regime in the presence of high amplitude pulse excitation. Authors introduced an OLED electrical model that identifies key design parameters [15]. This paper builds on this previous work and proposes an OLED electrical model that is further fine-tuned to reproduce the device electrical response to faster and shorter pulses than those reported in [15]. The model takes into account the physical characteristics and topology of the OLED.

A new and original ultra-fast OLED design with a topology that is optimized from the equivalent electric model key parameters is then presented as well as a coplanar waveguide electrodes complying with radio-frequency circuits and systems design rules. To demonstrate the effectiveness of the proposed design approach, this paper presents preliminary experimental measurements of the new OLED design, in the presence of an ultra-short pulse, in terms of electrical and optical responses.

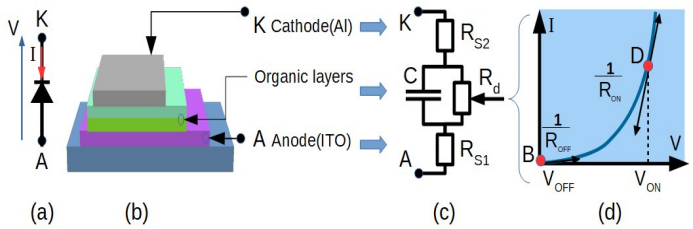


Figure 1: Equivalent electrical model of different part of OLED device.

## Equivalent electrical model:

The most commonly used simple equivalent electrical model for an OLED are not optimized for ON-OFF operation scheme with high amplitude of excitation [16,17]. The proposed equivalent electrical model, shown in Fig.1.c, is established from the OLED geometry/topology, shown on Fig.1.b, and its I-V characteristic, shown in Fig.1.d. Fig.1.b depicts a typical OLED geometry with a stacked structure of thin organic layers sandwiched between an indium tin oxide (ITO) anode, and a metallic (Al) cathode. From an electrical point of view, this structure is equivalent to a combination of several resistors and a capacitor. The resistors represent ohmic losses due to; firstly, the ITO sheet resistance (contact resistance $R_{S1}$), secondly, the low conductivity of each of the organic layers (bulk resistance $R_b$), and thirdly, the cathode resistance (contact resistance $R_{S2}$). The capacitive behavior results from the fact that the OLED is basically made of almost dielectric materials, i.e. the organic layers sandwiched between metallic plates (the electrodes). Additionally, the energy barriers between adjacent organic layers induce a junction capacitance. For the sake of simplicity, all the capacitors are included in a single equivalent capacitor C. The proposed equivalent electrical model elements are shown on Fig 1.c.

Typical I-V OLED curve is shown fig 1.d. In ON-OFF regime the operation points are B and D corresponding respectively to an excitation voltage $V_{OFF} = 0$ V (OFF-state) and to an excitation voltage $V_{ON} >> 0$ (ON state). The respective slopes of the I-V curve in B and D are:

$$\frac{1}{R_{OFF}} = \frac{dI}{dV}_{at\ V=V_{OFF}=0} \quad \text{and} \quad \frac{1}{R_{ON}} = \frac{dI}{dV}_{at\ V=V_{ON}} \qquad \text{Eq. (1)}$$

$R_{ON}$ being the effective resistance in the equivalent circuit while high excitation voltage is applied during the ON state. The higher the amplitude of excitation, the lower is $R_{ON}$ resistance. During the OFF state a similar reasoning applies except that the effective resistance $R_{OFF}$ is high enough to be considered as an open circuit. This is clearly shown by the slope of the I-V curve which is close to zero. In ON-OFF operation regime a dynamic resistor $R_d$ is used that is either equal to $R_{ON}$ or to $R_{OFF}$ depending on which state the OLED is switched to. In order to take the ON-OFF switching into account in the equivalent electrical circuit, we introduced the dynamical resistance $R_d$ which is the sum of the inverse of the slope of the I-V curve, and of the bulk resistor $R_b$ such that $R_d = R_{ON} + \mathbf{R_b}$ in ON state and $R_d = R_{OFF} + \mathbf{R_b}$ in the OFF state.

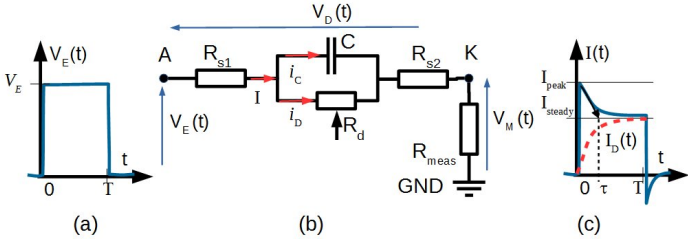


Figure 2: Electrical circuit for pulsed excitation of OLED

In order to measure the current I flowing through the OLED, a measurement resistor ($R_{meas}$) is connected in series with the device as shown on Fig. 2.b.

From the electrical excitation circuit shown in Fig. 2.b, the relationship between the OLED current I and the excitation voltage $V_E$ reads:

$$\frac{dI(t)}{dt}+\left(1+\frac{R_d}{R_{S1}+R_{S2}+R_{meas}}\right)\frac{1}{R_dC}I(t)= \frac{1}{R_{S1}+R_{S2}+R_{meas}}\left[\frac{dV_E(t)}{dt}+\frac{1}{R_dC}V_E(t)\right] \quad \text{Eq. (2)}$$

The current I flowing through $R_{meas}$ is the sum of $i_D$ and $i_C$ which are respectively the currents flowing through the diode and the junction capacitor C. The part of the current flowing through the dynamic resistor $R_d$ and not through the capacitance is then:

$$i_D(t)=\frac{V_E(t)-(R_{S1}+R_{S2}+R_{meas})I(t)}{R_d} \quad \text{Eq. (3)}$$

The ON-OFF operation regime is modeled with an analytical expression of the excitation voltage $V_E(t)$ defined as a gate function with a constant amplitude $V_E$, between 0 to T and with zero amplitude outside as shown Fig 2.a.

The current waveform I(t) flowing through the OLED, shown in Fig.2.c is then obtained by solving eq. 2 with $V_E(t)$ being replaced by its on-state value $V_E$ and its derivative by zero. For the sake of simplification we introduced the total serial resistance $R_{ST}=R_{S1}+R_{S2}+R_{meas}$ and consider only the rising flank of the solution (step function) of the differential equation eq. 2.

$$I(t)=\frac{1}{R_d+R_{ST}}\left[1+\frac{R_d}{R_{ST}}\exp\left(-\frac{R_d+R_{ST}}{R_{ST}}\frac{1}{R_dC}\,t\right)\right]V_E \quad \text{Eq. (4)}$$

Using eq. 3 and eq. 4, the effective current $I_D$ flowing through $R_d$ reads:

$$I_D(t)=\frac{1}{R_d+R_{ST}}\left[1-\exp\left(-\frac{R_d+R_{ST}}{R_{ST}}\frac{1}{R_DC}\,t\right)\right]V_E \quad \text{Eq. (5)}$$

*I(t)* starts with an initial turn-on peak current value $I_{peak}$ given by eq. 6 calculated in the particular case t=0.

$$I_{peak}=\frac{V_E}{R_{S1}+R_{S2}+R_{meas}}=\frac{V_E}{R_{ST}} \quad \text{Eq. (6)}$$

The current peak is followed by a decay toward a steady state value of I(t) reached for t larger than the decay time or for $t=+\infty$ given by eq. 7;

$$I_{steady}=I(t=+\infty)=\frac{V_E}{R_d+R_{ST}}=\frac{(R_{S1}+R_{S2}+R_{meas})}{R_d+(R_{S1}+R_{S2}+R_{meas})}I_{peak} \quad \text{Eq. (7)}$$

A more physical understanding of eq. 6 is revealed if at the onset of the pulse it is assumed that C is a short circuit and $R_d$ is infinite. Then, the equivalent electric circuit is reduced to the serial resistances $R_{ST}=R_{S1}+R_{S2}+R_{meas}$ and the current flowing through them when a voltage $V_E$ is applied at their terminals is indeed given by Ohm's law and eq.6.

Similar but different physical understanding holds for the expression of the steady-state current given by eq. 7; when C is fully loaded, its current stops, and C can be replaced by an open circuit in the equivalent circuit which reduces to the serial resistances $R_d+R_{ST}$. Consequently, the steady-state current is simply given by Ohm's law with voltage $V_E$ applied to the terminals of $R_d+R_{ST}$.

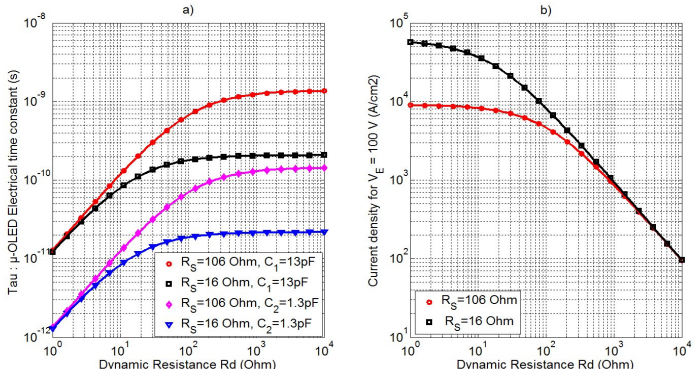


Figure 3: (a) µ-OLED Electrical time Constant and (b) Current density $J_D=I_D/S$ ($S=87x120\mu m^2$) for a 100 V excitation as a function of the dynamical resistance $R_d$ for $R_{ST1}=106\Omega$ and $R_{ST2}=16\Omega$ with $C_1$= 13 pF and $C_2$=1.3 pF.

Equations 6 and 7 indicate that reductions in the values of the serial resistors $R_{S1}$ and $R_{S2}$ as well as the dynamic resistor $R_d$ help to maximize the µ-OLED steady-state current which is the value towards which converges $I_D(t)$ the essential and unique contributing current to the light emission by the OLED (See fig. 2c).

The time constant τ (Eq.6) of the exponential decay is derived from the exponential term in eq. 4 and eq. 5 and reads as a function of the electrical model elements $R_{s1}$, $R_{s2}$, $R_{meas}$, $R_d$ and C:

$$\tau=\frac{C}{\frac{1}{R_d}+\frac{1}{R_{s1}+R_{s2}+R_{meas}}} \quad \text{Eq. (8)}$$

The electrical time response of the device, ie. the time needed for I(t) to decay from 90% to 10% of its peak value to its steady state value, (or for $I_D(t)$ to grow from 10% up to 90% of the steady state value) is simply $T_r = 2.2\,\tau$. From Eq. 8, it is clear that a first route to reduce the OLED time response is to minimize the capacitance C for example by reducing the active area surface S. Another route to reduce the value of $T_r$ is to reduce the values of resistors $R_d$, $R_{s1}$, $R_{s2}$, and $R_{meas}$. It is worth noting that to achieve $T_r$ minimization, both Rd and ($R_{ST}= R_{S1}+R_{S2}+R_{meas}$) must be minimized. Otherwise, $\tau \sim R_d C$ if $R_d << (R_{S1}+R_{S2}+R_{meas})$, or $\tau \sim (R_{S1}+R_{S2}+R_{meas})\,C$ if $R_d >> (R_{S1}+R_{S2}+R_{meas})$.

Figure 3 presents the OLED electrical time constant τ and the normalized current density as a function of the dynamic resistance $R_d$ for four different scenarios; In the first realistic scenario the measurement resistor $R_{meas}$ =50Ω and the serial resistors $R_{S1}$ and $R_{S2}$ are large resulting a total value $R_{ST1}=R_{S1}+R_{S2}+R_{meas}=106\ \Omega$ while the capacitance $C_1$=13pF. The choice of these model parameters values is based on previous measurements reported in [15]. In the second more optimistic scenario, all the serial resistors $R_{S1}$ and $R_{S2}$ have been minimized via metallization of the ITO and the measurement resistor is set to $R_{meas}=10\ \Omega$ resulting in $R_{ST2}=16\Omega$. The capacitance remains $C_1$=13pF. The third and fourth scenarios correspond respectively to $R_{ST1}=106\Omega$ and $C_2$=1.3pF and $R_{ST2}=16\ \Omega$ with $C_2$=1.3pF which are very optimistic scenarios with a tenfold reduction of the µ-OLED capacitance.

In figure 3.a the electrical time constant function saturates to $\tau_1$=1.36ns in the first scenario case ($R_{ST1}=106\ \Omega$ -red line with circles) whereas it saturates to $\tau_2$=206 ps in the second case with $R_s=16\ \Omega$ (black lines with squares). In the third and fourth scenarios the electrical time constant saturates respectively to $\tau_3$= 142 ps and $\tau_4$=22 ps. In any case, decreasing $R_d$ below $R_{ST}$ will reduce further the time constant. With these small values of the electrical time constants, this numerical analysis provide preliminary indications on the possibility to design optoelectronic organic devices one or more order of magnitude faster than what has been reported so far in the literature. Moreover, these low values of the electrical time constants being available for a large range of the dynamic resistance $R_d$. This

indicates that high excitation level (low $R_d$ values) is not compulsory

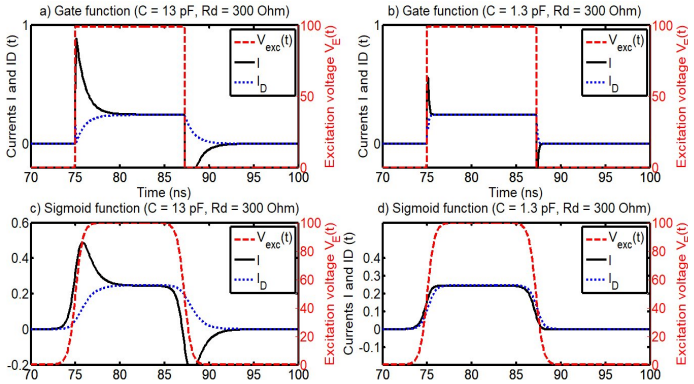


Figure 4: Simulations showing the electrical response of a µ-OLED to a ~10ns pulse excitation based on the differential equation 2 and on equation 3. The different simulations were runned with $R_d = 300\ \Omega$, with different capacitance values ($C = C_1 = 13$ pF left column and $C = C_2 = 1.3$ pF right column), and with different shapes of the electrical excitation signal (upper figures with gate functions, lower figures with sigmoïd functions). Continuous black traces correspond to the total current I while dotted blue lines correspond to the part $I_D$ of the current flowing through the organic hetero-structure and that produces the emission of light. In a) and b) the excitation (red stripped line) is a gate function, whereas in c) and d) the excitation function is a sigmoïd In a) and c) the time constant is $\tau_1 = 1$ ns ($C_1 = 13$ pF). In b) and d) the time constant are $\tau_2$=100 ps ($C_2 = 1.3$ pF).

to achieve high-speed behavior in organic optoelectronic devices.

In fig 3.b the current density is evaluated as a function of $R_d$. The maximum current density achievable with low $R_d$ values is limited by the serial resistance ($R_{ST}$=$R_{S1}$+$R_{S2}$+$R_{meas}$) to 10 kA/cm$^2$ in the first scenario and to ~50kA/cm$^2$ in the second one. Note that with $R_{ST1} = 106\ \Omega$ and $R_d = 300\ \Omega$, which constitute realistic conditions, the maximum current is to be limited by $I_D/S = 2.1$ kA/cm$^2$. To minimized $R_d$, the operating point D (Fig 1) is to be moved up along the I-V curve by increasing $V_{ON}$, whereas to minimized ($R_{ST} = R_{S1}+R_{S2}+R_{meas}$) the device is to be modified physically; $R_{S1}$ can be minimized via the metallization of the part of the ITO that is not the active area, $R_{S2}$ can be minimized with a thicker aluminum deposition and with shorter electrical track. Finally $R_{meas}$ can simply be set to the minimum resistance value that still allows a noise limited measurement of the $V_M(t)$ voltage taking into account the sensitivity of the measurement equipment. Note however that the turn-on peak current $I_{peak}$ increases with the value of the total resistance $R_{ST}$ and actually will tend to infinity if $R_{ST}$ is to be zero. In practice this means a destruction of the OLED. Also, note that the steady current $I_{steady}$ tends to the peak current $I_{peak}$ when $R_d << (R_{S1}+R_{S2}+R_{meas})$ as illustrated from fig. 4.b. This is likely going to result to; firstly to a maximization of the expected steady state current and secondly to a beneficial mitigation of the transient effects.

The analysis of the analytical expressions can therefore be summarized into three design guidelines; 1) reducing the OLED active area, 2) minimizing the serial resistance and 3) operating with amplitude pulses high enough to obtain a dynamical resistance $R_d$ smaller than the total of the serial resistances $R_{ST}$ and to access operation regime with smaller difference between $I_{steady}$ and $I_{peak}$.

## Numerical results

The differential equation (Eq. 2) is solved numerically using Runge-Kutta 2$^{nd}$ and 3$^{rd}$ order method using different excitation functions, different values of the capacitance C. The current $I_D(t)$ flowing through the active part of the µ-OLED is then deduced. Results are shown fig. 4 in the case of gate excitation function (upper figures in Fig. 4) and sigmoïd excitation function (lower figures in fig. 4) with a 10ns duration.

In the case of a gate excitation function (Fig 4.a and b), the beginning and the end of the pulse response exhibit overshoots indicating the charge and the discharge of the C capacitance. As expected, the overshoots become less pronounced in duration when the capacitance C decreases from $C_1$=13 pF to $C_2$=1.3 pF, which corresponds to the decrease of the electrical time constant $\tau_e$ (Eq. 5). In the case of a sigmoïd excitation function (Fig 4.c and d) the overshoot is not visible for the smaller value of the time constant ($R_d = 300\Omega$, $C = 1.3$ pF). We would like to emphasize that the absence of overshoot is not an evidence of slow response. Note that whatever the excitation function is, the $I_D$ current does reach its maximum (stationary state) before the end of the pulse duration. A first conclusion is that the excitation function has a large impact on the discharge and therefore the estimation of the µ-OLED time constant from the measurement of the capacitance discharge is to be considered cautiously. Moreover, the current $I_D$ reaches its steady value faster with the gate excitation function than with the sigmoid. For this reason, it is important to preserve the integrity of the excitation signal. This can be done among other things by minimizing the parasitic reflection resulting from impedance mismatch. Here we propose to improve the impedance matching between µ-OLED electrodes and wires coming from a pulse generator with feeder line electrodes.

## OLED circuit design

Operating OLEDs in ON/OFF mode means driving them with pulses. In the presence of ultra-short pulses, the driving signal contains high frequency components and issues such as impedance matching must be taken into account. Indeed, when voltage impulse of few nanoseconds is applied to an OLED, part of its energy is reflected (not absorbed by/delivered to the OLED) if there is any impedance mismatch between the feeding line and the device or anywhere in the driving circuit. The amount of reflected energy is quantified by the reflection coefficient that is defined by:

$$\Gamma = \frac{Z_D - Z_C}{Z_D + Z_C} \quad \text{Eq. (9)}$$

where $Z_D$ is the equivalent impedance of the device and $Z_C$ is the characteristic impedance of the line. Reflection has also the effect of distorting pulse waveforms which makes it difficult to even estimate the response time of the device has mentionned previously. To avoid as much as possible undesired effects, we applied two modifications on the ITO electrode; we propose for the first time in the OLED technology to integrate both part of the driving circuit and the matched feeding lines onto the ITO thin film coating the glass substrate [18]. More specifically, OLED electrode dimensions and shape will be modified to become coplanar waveguide feeding lines.

Coplanar waveguide (CPW) has been chosen to design the new pattern of OLED electrodes because it requires only one side of the substrate covered with conductive material contrary to micro-strip configuration. It is thus easily and quickly adaptable to current OLED substrates. The dimensions of the feeding lines are calculated to obtain a characteristic impedance $Z_c$ equal to 50 Ω at the $F_b$=1GHz base frequency (knowing that 98% of the pulse spectrum energy lie in frequency range from 0 to $5F_b$).

CPW line was described for the first time by C. WEN[19], but it is applied to design ultra-fast organic optoelectronic devices for the first time. It consists of a strip of thin conductive strip on the surface of a dielectric with two ground planes running adjacent and parallel to the strip as shown on fig. 5.

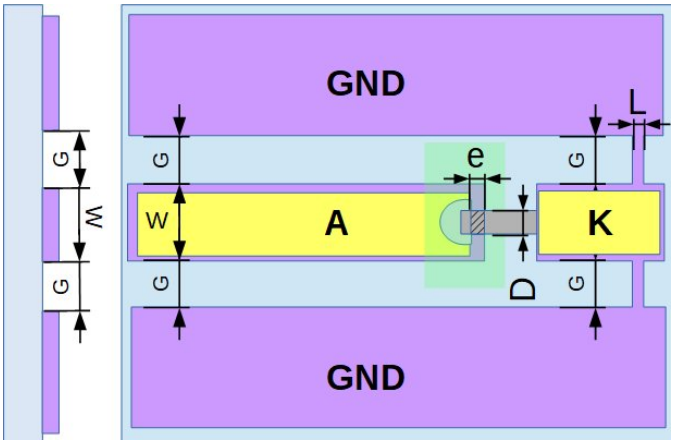


Figure 5: Structure of a µ-OLED on ITO with coplanar waveguide electrodes as feeder line an integrated measurement resistances. (GND:Ground plane), A: Anode K; Cathode) (ITO: Purple, Gold : Yellow, Aluminum: Grey , light blue: glass substrate)

Figure 5 illustrates the CPW structure where H and $\varepsilon_r$ are respectively the thickness and the relative dielectric permittivity of the dielectric material which is a glass substrate used in this work. W and T are the width and thickness of the central strip respectively whereas G is the width of the gap on either sides between the central strip and the ground planes. With a W=1000µm width ITO central anode separate by a gap G=243µm from the ITO ground planes on a H=700µm thick glass substrate with relative permittivity $\epsilon_r=7.75$ a $Z_C=50\,\Omega$ characteristic impedance is obtained.

CPW is compatible with the integration of electrical elements of the driving circuit onto the substrate as close as possible to the OLED so as to reduce the effect of parasitic reflections and preserve the shape of the fast electrical excitation pulses.

In the current work, integrating the electrical driving circuit reduces to the addition of a built-in measurement resistance $R_{meas}$. To integrate the latter onto the substrate, two thin stripes connecting the cathode to both ground planes with $R_{stripe} = 2 \times R_{meas}$ are added as illustrated in fig. 5. The width L of these stripes is simply calculated from the law of resistance with its length imposed by the gap G, with the section defined partially by the ITO thickness T=120 nm, and with the ITO resistivity $\rho_{ITO}$ :

$$L=\rho_{ITO}\frac{G}{2R_{meas}T} \qquad \text{Eq. (10)}$$

Practical dimensions for $R_{MEAS}=50\,\Omega$ are G=243µm and L=182µm.

## Experimental results and validation of the model

After fabrication, the samples are characterized electrically first under DC operation. The serial resistances exhibits $R_{S1} = 45\,\Omega$, $R_{S2} = 10\,\Omega$, $R_{meas} = 51\,\Omega$. The active area has been measured to S = 87 x 120µm$^2$, and the surface capacitance value of 124 nF/cm$^2$ at 0.5 Ghz estimated from a previous work with similar organic heterostructure has been used. The total serial resistance and the estimated capacitance $C_1$ = 13pF corresponds to scenario 1.

The Organic heterostructure is made with 30nm of m-MTDATA as hole injection layer (HIL), 10 nm-thick NPD as hole transport layer (HTL), 30 nm of Alq3 doped with DCM as a light emitting layer, 5nm of BCP as hole blocking layer (HBL), and 25 nm of Alq3 as electron transporting layer respectively ended with a LiF (1nm) /Al (120 nm) cathode layer.

In order to record the opto-electrical behaviour of the device, each OLED is placed on a response time measurement system consisting of a probe station (Cascade opto-PM5), a high pulse generator (AVTECH AVL-2A-B), and a digital oscilloscope (Tektronix TDS

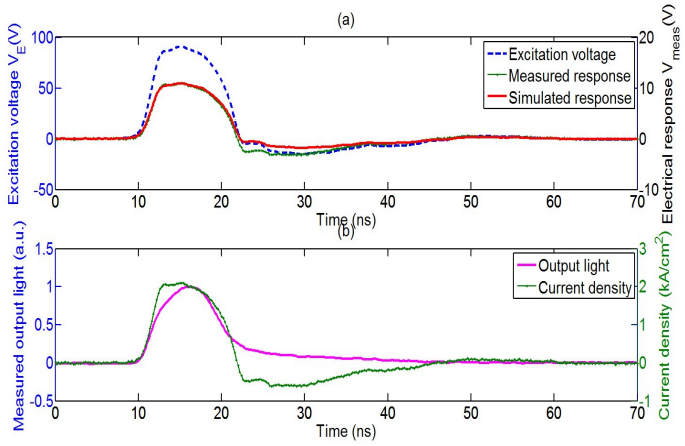


Figure 6: Time domain waveforms of electrical and optical response of the µ-OLED device for 9 ns pulse duration and an excitation amplitude of $V_E$=100V. a) Excitation $V_E(t)$ (blue stripped line), measured electrical response $V_M(t)$ (green line with dots) and simulated electrical response (red thick line) showing a good fit between the measurement and the simulation. b) Measured current density $J_D(t)$ (green thin line with dots) and the optical response (thick magenta line)).

7254). A 100 V amplitude excitation pulse with 10ns duration is delivered from the generator and applied to the device, while measurements are recorded with the digital oscilloscope. Current density response is measured across the built-in measurement resistance $R_{meas}$ using a GSG probe. Simultaneously, light output is collected from the bottom of the substrate into a NA=0.5 numerical aperture optical fibre connected to an avalanche photodiode with 400 MHz bandwidth (Thorlabs APD3040A2). All measurements are performed in an ambient atmosphere at room temperature.

Figure 6 presents both experimental results and simulations for the sake of comparison and validation of the model. More specifically, fig. 6.a presents the excitation voltage $V_E(t)$ (blue stripped line), the electrical response $V_M(t)$ (green line with dots) measured across the measurement resistance $R_{meas}$, and a simulation (red continuous line) performed with the measured excitation signal $V_E(t)$ (blue stripped line).

The measured excitation voltage $V_E(t)$ exhibits smooth flanks similar than those of the sigmoïd functions in fig. 4.c and d. Because of this and following the conclusions of the numerical analysis the electrical time constant can not be measured directly from the measured time trace, but rather from the parameters used for the fitting between the measurement and equation 2.

For these reasons and for the sake of comparison, the measured electrical response and electrical response simulated from equation 2 with $R_{ST1} = 106\,\Omega$, $R_d = 312\,\Omega$ (extracted by fitting), and $C_5$=1.4 pF (13.8nF/cm$^2$) are both plotted on the same figure. The electrical response $V_M(t)$ exhibits a pulse duration (FWHM) of 9.0 ns similar to that of the excitation which is a strong indication that the µ-OLED with CPW electrodes respond much faster than the pulse duration. Note that the parameters used for the fitting are very close to those involved in the third scenario since $R_{ST1}$ is the same, $R_d$=312Ω differs by 4% only and $C_5$=1.4pF differs by 7% from $C_2$. Clearly, the good qualitative fitting between the measurement and the simulation based on reasonable values of the electrical model validates the modelling in ON-OFF regime and demonstrates its relevancy. Based on this conclusion it appears safe to used the model to estimate the electrical time constant. From the electrical parameters values $R_{ST1} = 106\,\Omega$, $R_d = 312\,\Omega$, and $C_5$=1.4 pF, equation 6 provides an electrical response time of $\tau_e = 110\,ps$ .

This the first of the two strong indications that 50Ω impedance characteristic CPW electrodes are very beneficial to very-high speed µ-OLED.

Indeed, the electrical response to a pulse excitation of the µ-OLED with CPW electrodes $\tau_e = 110\,ps$ is two orders of magnitude lower than previously reported work with the same active area but without CPW electrodes ($\tau << 9.6$ ns±3.3ns) [15]. Such an almost adiabatic response explains why the electrical response exhibits the same pulse duration than the excitation.

A second indication of the benefit of the CPW electrodes is to compare the value of the capacitance and the surface capacitance of µ-OLED with and without CPW electrodes. The surface capacitance calculated from the ratio $C_5$ to S with $S = e \times D = 87 \times 120 \mu m^2$ is $C_5/S = 13.8 nF/cm^2$. It is tenfold smaller than that reported in the previous study [15], but in better agreement with other values reported in the literature in the range 20-40nF/cm² and in the MHz range [19]. The active area S being similar in the current experiment and in the experiment reported in [15], the main difference between both types of µ-OLED being the CPW feeding line electrodes, it confirms their role in the tenfold parasitic capacitance reduction. The capacity difference can be explained by the impedance mismatch along the electrical line with different characteristic impedance of the wires, cables, distant measurement resistance and device resulting in a total parasitic capacitance ten fold larger (124nF/cm²) when CPW is absent.

Figure 6.b presents the light output (continuous magenta trace) and the current density $J_D(t)=I_{D(t)}/S$ (green thin line with dots) calculated from eq. 3 using the measured voltage response $V_M(t)$ and the measured excitation voltage $V_E(t)$. The current density waveform exhibits a rising flank sharper than the falling flank although the pulse duration remains equal to the excitation pulse duration at 9.0ns. The peak value of the current density reaches 2.04 kA/cm² which is less than 3% different from the maximum current density value 2.1 kA/cm² calculated from equation 5 with $R_d = 312\,\Omega$ and very similar to what is plotted in fig. 3.b. This is an indication of the relevancy and the robustness of the model. The rise time of the $I_D(t)$ current from 10% to 90% of its maximum value is 2.1ns indicating that the device can be submitted to pulses shorter than 10ns with a still perceptible light response. Note again that the reason why the µ-OLED electrical rise time is different from $\sim \simeq 2.2\,\tau_e = 242\,ps$ is because the excitation signal is not a gate-like function.

Additionally, the current $I_D$ flowing through the organic hetero-structure is effectively converted into photons as proved by the ouput light emission (magenta trace in fig.6b). With 8.2ns and 3.6ns in duration and rise time respectively, the optical pulse exhibits smaller duration and slower rise time than that of the electrical pulse. A qualitative analysis of the light output shows that the optical trace increases exponentially up to the half of the duration of the current density pulse and decreases exponentially after it, confirming that the measured optical response is slower than the electrical response. Further investigation with a faster photodiode is required to check whether or not the measurement is not limited by the photodiode response time.

# Conclusion and perspectives:

The current study proposes a model for high speed µ-OLED in ON-OFF pulse excitation regime that is successfully validated with measurements. The coplanar waveguide electrodes made of ITO on glass substrates compatible with $S = 87 \times 120 \mu m^2$ µ-OLED and with 50Ω integrated measurement resistance lead to tenfold smaller capacitance values, and two orders of magnitude faster electrical response down to $\tau = 110\,ps$ . The combination of preliminary measurements and simulation demonstrated the interest of the proposed design for the reduction of the µ-OLED electrical time response under ultra short pulse excitation scheme. This work shows successful generation of perceptible light response under better than state-of-the-art ultra short electrical pulse duration of 9ns, 2.1ns rise-time. It demonstrates not only pulse duration in the range of the radiative lifetime of singlet excitons, but also that the OLED device can sustain state of the art current density up to 2kA/cm² without heat breakdown.

As perspectives, the metallization of the electrodes can lead to a further decreases of the serial resistance and therefore to a further decrease of the electrical time response down to 20 ps and to current density up to 3 kA/cm² in the case of an excitation amplitude of 100V. The next step will be to quantify precisely the true light intensity emitted by the OLED to investigate the optical excitation density as steps forwards towards the resolution of the electric excitation issue of the organic diode laser.

A. C. Chime, A. P. A. Fischer, M. Chakaroun, H. Nkwawo, (*Université Paris 13, Sorbonne Paris Cité, Laboratoire de Physique des Lasers UMR CNRS 7538, 93430 Villetaneuse, France*)

A. P. A. Fischer, (Centrale de Proximité en Nanotechnologies de Paris Nord) *Université Paris 13, Sorbonne Paris Cité, Villetaneuse, France*)

S. Bensmida (*Communication Systems and Networks Group, Merchant Venturers School of Engineering, University of Bristol, MVB Bld, Woodland Rd, Bristol, BS8 1UB, UK*)

A. C. Chime (*Institut Universitaire de Technologie FOTSO Victor, Université de Dschang, Cameroun*)

E-mail: Fischer@iutv.univ-paris13.fr

***References***

1 D. Kasemann, R. Brückner, H. Fröb, and K. Leo, “Organic light-emitting diodes under high currents explored by transient electroluminescence on the nanosecond scale,” Physical Review B, vol. 84, no. 11, Sep. 2011.

2 I. D. W. Samuel and G. A. Turnbull, “Organic Semiconductor Lasers,” Chemical Reviews, vol. 107, no. 4, pp. 1272–1295, Apr. 2007.

3 H. Yamamoto, T. Oyamada, H. Sasabe, and C. Adachi, “Amplified spontaneous emission under optical pumping from an organic semiconductor laser structure equipped with transparent carrier injection electrodes,” Applied Physics Letters, vol. 84, no. 8, pp. 1401–1403, Feb. 2004.

4 H. Nakanotani, N. Matsumoto, H. Uchiuzou, M. Nishiyama, M. Yahiro, and C. Adachi, “Very low amplified spontaneous emission threshold and electroluminescence characteristics of 1,1′-diphenyl substituted fluorene derivatives,” Optical Materials, vol. 30, no. 4, pp. 630–636, Dec. 2007.

5 H. Nakanotani, H. Sasabe, and C. Adachi, “Singlet-singlet and singlet-heat annihilations in fluorescence-based organic light-emitting diodes under steady-state high current density,” Applied Physics Letters, vol. 86, no. 21, p. 213506, May 2005.

6 M. A. Baldo, R. J. Holmes, and S. R. Forrest, “Prospects for electrically pumped organic lasers,” Physical Review B, vol. 66, no. 3, Jul. 2002.

7 C. Gartner, C. Karnutsch, C. Pflumm, et U. Lemmer, « Numerical Device Simulation of Double-Heterostructure Organic Laser Diodes Including Current-Induced Absorption Processes », IEEE Journal of Quantum Electronics, vol. 43, no 11, p. 1006-1017, nov. 2007.

8 A. J. C. Kuehne and M. C. Gather, “Organic Lasers: Recent Developments on Materials, Device Geometries, and Fabrication Techniques,” Chemical Reviews, vol. 116, no. 21, pp. 12823–12864, Nov. 2016.

9 H. Nakanotani, T. Oyamada, Y. Kawamura, H. Sasabe, and C. Adachi, “Injection and transport of high current density over 1000 A/cm2 in organic light emitting diodes under pulse excitation,” Japanese journal of applied physics, vol. 44, no. 6R, p. 3659, 2005.

10 S. Schols, L. Van Willigenburg, S. Steudel, J. Genoe, and P. Heremans, “Pulsed Excitation of OLEDs With a Remote Metallic Cathode,” IEEE Journal of Quantum Electronics, vol. 46, no. 1, pp. 62–67, Jan. 2010.

11 N. C. Giebink and S. R. Forrest, “Temporal response of optically pumped organic semiconductor lasers and its implication for reaching threshold under electrical excitation,” Physical Review B, vol. 79, no. 7, Feb. 2009.

12 Zhang, M. Whited, M. E. Thompson, and S. R. Forrest, “Singlet–triplet quenching in high intensity fluorescent organic light emitting diodes,” Chemical Physics Letters, vol. 495, no. 4–6, pp. 161–165, Aug. 2010.

13 B. Wei, M. Ichikawa, K. Furukawa, T. Koyama, and Y. Taniguchi, “High peak luminance of molecularly dye-doped organic light-emitting

diodes under intense voltage pulses," Journal of Applied Physics, vol. 98, no. 4, p. 44506, Aug. 2005.

14 V. G. Kozlov et al., "Structures for organic diode lasers and optical properties of organic semiconductors under intense optical and electrical excitations," IEEE Journal of Quantum Electronics, vol. 36, no. 1, pp. 18–26, 2000.

15 L. Zeng et al., "Electrical and optical impulse response of high-speed micro-OLEDs under ultrashort pulse excitation," IEEE Transactions on Electron Devices, vol. 64, no. 7, pp. 2942–2948, Jul. 2017.

16 S. H. Kim et al., "Impedance spectroscopy of single- and double-layer polymer light-emitting diode," Journal of Applied Physics, vol. 87, no. 2, pp. 882–888, Jan. 2000.

17 Joon-ho Ahn, Dong-Hoe Chung and Joon-Ung Lee, "Equivalent-Circuit Analysis of Organic Light-Emitting Diodes by Using the Frequency-Dependent Response of an ITO/Alq3/Al Device," in Journal of the Korean physical society; vol. 46, no. 2, pp. 546–550, Feb. 2005.

18 W. Hilberg, "From approximations to exact relations for characteristic impedances," IEEE Transactions on Microwave Theory and techniques, vol. 17, no. 5, pp. 259–265, 1969.

19 C. P. Wen, "Coplanar waveguide: A surface strip transmission line suitable for nonreciprocal gyromagnetic device applications," IEEE Transactions on Microwave Theory and Techniques, vol. 17, no. 12, pp. 1087–1090, 1969.

20 G. Garcia-Belmonte, H. J. Bolink, et J. Bisquert, « Capacitance-voltage characteristics of organic light-emitting diodes varying the cathode metal: Implications for interfacial states », Physical Review B, vol. 75, no 8, feb. 2007.